LETTER

doi:10.1038/nature10863

Goblet cells deliver luminal antigen to CD103$^+$ dendritic cells in the small intestine

Jeremiah R. McDole[1]*, Leroy W. Wheeler[2]*, Keely G. McDonald[2], Baomei Wang[1], Vjollca Konjufca[3], Kathryn A. Knoop[2], Rodney D. Newberry[2] & Mark J. Miller[1]

The intestinal immune system is exposed to a mixture of foreign antigens from diet, commensal flora and potential pathogens. Understanding how pathogen-specific immunity is elicited while avoiding inappropriate responses to the background of innocuous antigens is essential for understanding and treating intestinal infections and inflammatory diseases. The ingestion of protein antigen can induce oral tolerance, which is mediated in part by a subset of intestinal dendritic cells (DCs) that promote the development of regulatory T cells[1]. The lamina propria (LP) underlies the expansive single-cell absorptive villous epithelium and contains a large population of DCs (CD11c$^+$ CD11b$^+$ MHCII$^+$ cells) comprised of two predominant subsets: CD103$^+$ CX$_3$CR1$^-$ DCs, which promote IgA production, imprint gut homing on lymphocytes and induce the development of regulatory T cells[2–9], and CD103$^-$ CX$_3$CR1$^+$ DCs (with features of macrophages), which promote tumour necrosis factor-α (TNF-α) production, colitis, and the development of T$_H$17 T cells[5–7,10]. However, the mechanisms by which different intestinal LP-DC subsets capture luminal antigens *in vivo* remains largely unexplored. Using a minimally disruptive *in vivo* imaging approach we show that in the steady state, small intestine goblet cells (GCs) function as passages delivering low molecular weight soluble antigens from the intestinal lumen to underlying CD103$^+$ LP-DCs. The preferential delivery of antigens to DCs with tolerogenic properties implies a key role for this GC function in intestinal immune homeostasis.

We examined the *in vivo* antigen acquisition behaviour of intestinal LP-DCs in fluorescent DC-reporter mice using two-photon microscopy (Supplementary Fig. 1a). The intestine is imaged within the peritoneal cavity and images can be acquired from either the intact intestinal serosa or from the luminal surface through a small longitudinal incision in the intestine (Fig. 1a, b and Supplementary Movie 1, upper panels). The preparation is sufficiently stable to permit three-dimensional imaging of DC behaviour deep within intestinal tissues (Fig. 1c and Supplementary Movie 1, lower left panel) and preserves blood flow and epithelial barrier integrity for more than 4 h of continuous imaging.

We assessed antigen distribution by two-photon microscopy following the intraluminal injection of 10 kDa rhodamine dextran as a model antigen. Dextran coated the surface of the epithelium and filled the space between villi and crypts (Fig. 1a, b). In addition, we observed cylindrical dextran columns approximately 5 μm in diameter and about 20 μm long projecting through the villus epithelium and into the LP, when imaging from either serosal or luminal orientations (Fig. 1a–c, Supplementary Fig. 1b and Supplementary Movie 1, upper panels and lower right panel). Transepithelial dextran columns were common throughout the small intestine from duodenum to ileum, but did not cause a general disruption of the epithelial barrier as shown by the exclusion of dextran from the LP (Fig. 1a–c). We did not detect transepithelial dextran columns in the stomach, caecum, or colon, with the exception of the epithelium overlying the caecal patches (Supplementary Fig. 1c–e and Supplementary Movie 2). Confocal microscopy revealed that dextran columns were a subset of epithelial cells containing intracellular dextran, which had a continuous border of e-cadherin on their basolateral surface and were often in contact with yellow fluorescent protein (YFP$^+$) cells in the LP of CD11c-YFP reporter mice[30] (Fig. 1d, e and Supplementary Movie 4, right panel).

Periodic acid–Schiff staining of mucin in sections of the small intestine (Fig. 2a) produced a goblet cell (GC) staining pattern similar in frequency, distribution and dimensions to the dextran columns identified by two-photon microscopy (Fig. 2b, c). Furthermore, in contrast to the acellular and impermeable discontinuities seen in the small intestine epithelium[11], dextran columns were associated with a nucleus (Fig. 2d, Supplementary Fig. 2a and Supplementary Movie 3). To determine if the dextran-filled cells were in fact GCs, sections of intestine from mice given lysine-fixable dextran were stained with antibodies to mucin 2 (MUC2) and cytokeratin 18, which are both highly expressed by GCs[12]. Dextran columns showed near perfect colocalization with MUC2$^+$ and cytokeratin 18$^+$ epithelial cells displaying GC morphology (Fig. 2e, f). Therefore, we term this phenomenon 'goblet-cell-associated antigen passages' (GAPs). To address the possibility that GAPs are apoptotic GCs, we co-stained for various markers of apoptosis, including cleaved cytokeratin 18, cleaved caspase 3 and TdT-mediated dUTP nick end labelling (TUNEL; Supplementary Fig. 3a–i). In all cases, we found no association between apoptotic GCs and GAPs. Moreover, GAPs are distinct from villous M cells, because they did not colocalize with the M-cell marker glycoprotein 2 (GP2) (Fig. 2g)[13]. The frequency and distribution of GAPs assessed by two-photon microscopy was similar in all strains of specific-pathogen-free (SPF) mice examined (Supplementary Fig. 2b–d), with a non-significant trend toward more GAPs detected in the terminal ileum (Supplementary Fig. 2h). GAPs were also evident in human jejunum resection specimens (Fig. 2h, i), suggesting that GAPs are a general phenomenon of the healthy small intestine. We examined the frequency of GAPs in C3H/HejBir IL-10$^{-/-}$ mice[14], which develop spontaneous intestinal inflammation with GC loss, and in germ-free mice that lack normal gut flora. The number of GAPs and GCs correlated strongly; GAPs and GCs were significantly more numerous in germ-free mice (Supplementary Fig. 2e, g) and significantly fewer in IL-10$^{-/-}$ mice (Supplementary Fig. 2f, g).

Previous studies have shown that LP-DCs can extend transepithelial dendrites (TEDs) between intestinal epithelial cells to sample luminal contents and microbiota[15–18]. However, these studies used *ex vivo* and exteriorized tissue preparations that involved removing the luminal contents and mucous before imaging. Using our *in vivo* imaging preparation and confocal microscopy, we found that although LP-DCs probed the epithelium actively with their dendrites (Fig. 1c and Supplementary Movie 1, lower left panel, and Supplementary Movie 4), they did not extend TEDs into the intestinal lumen to capture fluorescent antigen in healthy mice (based on over 50 independent intravital imaging experiments examining all regions of the small intestine from the tip of the

[1]Department of Pathology and Immunology, Washington University School of Medicine, St Louis, Missouri 63110, USA. [2]Department of Internal Medicine, Washington University School of Medicine, St Louis, Missouri 63110, USA. [3]Department of Microbiology, Southern Illinois University, Carbondale, Illinois 62901, USA.
*These authors contributed equally to this work.

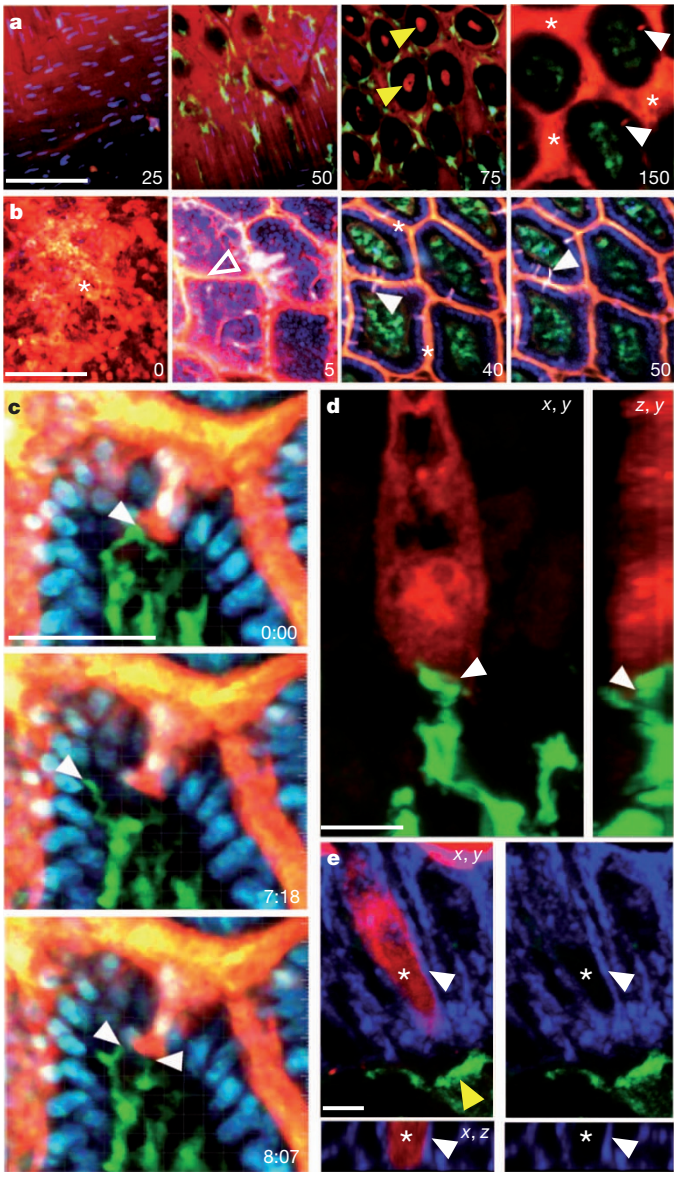

Figure 1 | Steady-state transepithelial delivery of luminal material in the mouse small intestine. **a**, **b**, Intestines from anaesthetized CD11c-YFP reporter mice injected intraluminally with 10 kDa dextran (red) imaged with intravital two-photon microscopy from the (**a**) serosal or (**b**) luminal surfaces. Optical sections at increasing depths (shown in μm) revealed dextran in the lumen (asterisks), the crypts (yellow arrows), on the epithelial surface (unfilled arrow) and columns of dextran that traversed the epithelium (white arrows). Dextran was generally excluded from the LP as identified by CD11c-YFP$^+$ LP-DCs (green) below the DAPI-stained epithelial nuclei (blue in **b**). Scale bars, 100 μm. **c**, Time-lapse recording of an LP-DC dendrite (green, white arrow) making repeated contacts with a dextran column (red) crossing the epithelium (DAPI-stained nuclei, blue). Scale bar, 50 μm; time stamp shows min:s elapsed time from the start of imaging. **d**, Rendered confocal image of a CD11c-YFP$^+$ DC (green) in contact with a dextran-filled epithelial cell (red). Panels show orthogonal views, contact is indicated by the white arrow. Scale bar, 5 μm. **e**, Confocal image of a dextran-containing cell (red) bordered by a continuous e-cadherin-positive (blue) surface (white arrow). Asterisk indicates the position of an optical section near the cell's centre showing intracellular dextran. A CD11c-YFP$^+$ DC (green, yellow arrow) is positioned near the base of the epithelium. Orthogonal projection (bottom panels); red channel removed (right panels). Scale bar, 5 μm.

villi to the base of the crypts). To confirm that our imaging approach can readily detect TEDs, we imaged CD11c-YFP reporter mice challenged with *Salmonella typhimurium*, which has been shown to upregulate TED formation[15]. Although rare LP-DC TEDs were observed in approximately 2% of villi, TEDs did not mediate the uptake of luminal dextran or beads on the basis of fluorescence colocalization (Supplementary Fig. 4a and Supplementary Movie 5, upper left panel).

Next, we examined whether paracellular leak[19] could serve as a major source of luminal antigen for small intestine LP-DCs. The intraluminal injection of 5 mg of 10 kDa dextran produced a faint 'feather'-like staining pattern between villous epithelial cells, consistent with paracellular leak (Supplementary Fig. 4b and Supplementary Movie 5, upper right panel). Time-lapse two-photon imaging showed that dextran collected at the base of the epithelium, but was flushed out of the villi efficiently during contraction and did not remain colocalized with LP-DCs even in areas of extensive paracellular leak (Supplementary Fig. 4b and Supplementary Movie 4, left panel, and Supplementary Movie 5, upper right panel). In addition, we did not detect paracellular leak around GAPs in fixed sections by confocal microscopy, despite the more permissive tight junctions of GCs[20]. However, we cannot exclude the possibility that LP-DCs capture low levels of antigen via paracellular leak, because this process might be below the level of detection of our imaging approach.

In contrast to TEDs and paracellular leak, two-photon time-lapse imaging provided direct evidence that GAPs are a source of luminal antigen for LP-DCs. In addition to dextran (Fig. 3a), GAPs were capable of transporting protein antigens (Fig. 3b). Although most GAPs remained visible for the duration of our imaging experiments, they were a dynamic phenomenon (Supplementary Movie 5, lower panels). Moreover, the manner in which LP-DCs interacted with GAPs varied. In some cases, DCs made stable contacts and slowly collected antigen over several minutes (Fig. 3a and Supplementary Movie 5, lower left panel) whereas in others, DCs actively probed GAPs and captured clumps of antigen (Fig. 3b and Supplementary Movie 5, lower right panel). We assessed the molecular weight exclusion limit of GAPs and found that beads ranging from 0.02 to 1.0 μm in size did not enter GAPs (Supplementary Fig. 4c). In contrast, GAPs filled rapidly with 10 kDa dextran (Supplementary Fig. 4d) and dextran colocalized with CD11c-YFP$^+$LP-DCs 2 h after intraluminal injection (Fig. 3a and Supplementary Movie 5, lower left panel). GAPs also filled with larger dextrans (Supplementary Fig. 4d); however, capture by LP-DCs was markedly reduced with 70 kDa dextran and undetectable with 2,000 kDa dextran during our 4-h imaging window.

The small intestine LP contains two prominent DC populations: CX_3CR1^- $CD103^+$ DCs with tolerogenic potential and CX_3CR1^+ $CD103^-$ DCs that have features of macrophages and have been implicated in intestinal inflammation[5–10]. We visualized LP-DC subsets *in vivo* using dual-reporter mice created by crossing CD11c-YFP mice with CX_3CR1-GFP knock-in mice (ref. 28) in which $CD103^-$ and $CD103^+$ LP-DCs can be distinguished by the presence or absence of CX_3CR1-GFP expression, respectively (Fig. 3c and Supplementary Fig. 5). We frequently observed CD11c-YFP$^+$ CX_3CR1-GFP$^-$LP-DCs sampling GAPs by two-photon microscopy, but this behaviour was rare in CD11c-YFP$^+$ CX_3CR1-GFP$^+$LP-DCs (Fig. 3c and Supplementary Fig. 6c); out of 50 total LP-DCs containing dextran, 49 were CD11c-YFP$^+$ CX_3CR1-GFP$^-$. Furthermore, when we directly observed antigen transfer from GAPs to DCs (20 out of 500 GAPs examined), GAPs delivered antigen exclusively to CD11c-YFP$^+$ CX_3CR1-GFP$^-$ LP-DCs (Fig. 3d). Immunofluorescence microscopy confirmed that the cells interacting with GCs were $CD103^+$ $CD11c^+$ LP-DCs and not $B220^+$ plasmacytoid DCs (pDCs) (Supplementary Fig. 6a). Moreover, flow cytometry showed that luminal antigen was captured preferentially by $CD103^+$ DCs at a proportion of roughly 10:1 over $CD103^-$ DCs (Fig. 3e) and rarely colocalized with pDCs (Supplementary Fig. 6b), consistent with the sampling bias observed by two-photon imaging. Control experiments demonstrated that antigen uptake during cell isolation was negligible (Supplementary Fig. 7), thus the flow cytometry results measure the *in vivo* antigen acquisition capacity of different LP-DC subsets. Interestingly, $CD103^+$ LP-DCs, but not $CD103^-$ LP-DCs, often stained positive for cytokeratin 18 (Fig. 3f and g), which is highly expressed by villous GCs (Fig. 3h).

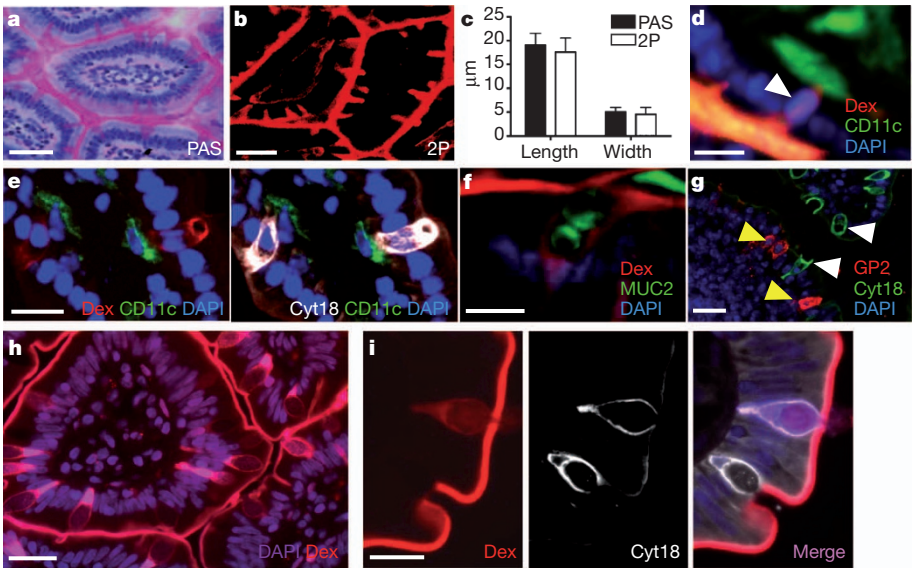

Figure 2 | GCs are associated with the transepithelial passage of luminal material. **a**, **b**, Periodic acid–Schiff (PAS) staining of GCs (**a**) and dextran columns (**b**) visualized by two-photon microscopy. **c**, PAS and dextran stained structures have similar morphology and dimensions. **d**, Dextran columns were often associated with a nucleus (white arrow). **e**, **f**, Dextran columns (Dex, red) colocalized with GC markers cytokeratin 18 (Cyt18, white) (**e**) and MUC2 (**f**). **g**, Cytokeratin 18-positive cells (white arrows) did not colocalize with the M-cell marker GP2 (yellow arrows). **h**, **i**, Dextran columns were present in healthy human small intestine (**h**) and stained positive for cytokeratin 18 (**i**). Scale bars, 30 µm (**a**, **b** and **h**), 20 µm (**d**, **e**, **g** and **i**), and 10 µm (**f**). Error bars, s.d.

Because cytokeratin 18 expression is undetectable in LP-DCs by quantitative real-time PCR (Fig. 3h), this suggests that CD103$^+$ LP-DCs interact selectively with GAPs and can capture GC-derived proteins.

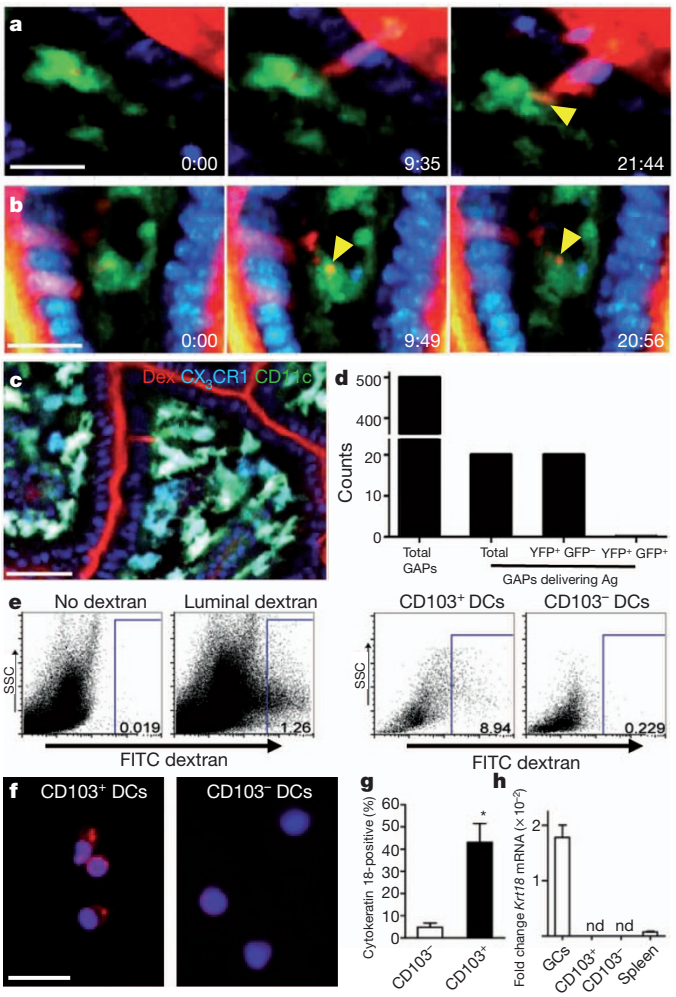

In two-photon imaging experiments, LP-DCs captured fluorescent luminal ovalbumin (Ova) readily from GAPs (Fig. 4a and Supplementary Movie 6), similarly to fluorescent dextran and BSA. To determine if LP-DCs could process and present luminal antigen, we administered Ova *in vivo*, then sorted LP-DCs and co-cultured them with OTI T cells[21]. T-cell proliferation was assessed on day 3 by both CFDA (dye) dilution (Fig. 4b, c) and by counting T cells after culture (Fig. 4d). Total LP-DC populations (CD45$^+$, CD11c$^+$, MHCII$^+$) were capable of inducing modest OTI T-cell proliferation that was significantly greater than controls (Fig. 4b, d). CD103$^+$ LP-DCs stimulated significant OTI T-cell proliferation, whereas CD103$^-$ LP-DCs from the same mice did not (Fig. 4d). The failure of CD103$^-$ LP-DCs to stimulate T cells was not due a lack of intrinsic antigen presentation capacity, because they were capable of inducing comparable levels of OTI T-cell proliferation to CD103$^+$ LP-DCs (81.4% to 88.2%, respectively) when Ova was added to the cell culture (Fig. 4c). These findings suggest that CD103$^+$ LP-DCs have cross-presentation capacity, similar to their mesenteric lymph node counterparts[2].

In some two-photon time-lapse recordings we observed GAPs forming or disappearing (Supplementary Movies 3 and 5, lower panels), suggesting that GAP formation could be related to changes in GC function or secretion. To test whether GC secretion was associated with GAP

Figure 3 | GAPs deliver soluble antigen to CD103$^+$ LP-DCs in the steady state. **a**, **b**, Time-lapse two-photon imaging of model antigens (red) dextran (**a**) and bovine serum albumin (BSA) (**b**) delivered by GAPs to LP-DCs (green, CD11c-YFP). Antigen from GAPs colocalized with LP-DCs (yellow arrows) over time. **c**, Two-photon imaging of CD11c-YFP CX_3CR1-GFP mice. GAPs (red) delivered antigen preferentially to CD103$^+$ LP-DCs (CD11c-YFP$^+$ CX_3CR1-GFP$^-$; green) over CD103$^-$ LP-DCs (CD11c-YFP$^+$ CX_3CR1-GFP$^+$; cyan) LP-DCs. **d**, Enumeration of GAPs and GAPs delivering antigen to LP-DC subtypes in CD11c-YFP CX_3CR1-GFP mice in two-photon recordings. **e**, Flow cytometry of LP cells showed that CD103$^+$ DCs captured more luminal dextran than CD103$^-$ DCs. FITC, fluorescein isothiocyanate. SSC, side scatter. **f**, Cytospins on sorted LP-DCs stained with DAPI (blue) and the GC marker cytokeratin 18 (red). **g**, Significantly more CD103$^+$ LP-DCs than CD103$^-$ LP-DCs stained cytokeratin 18-positive per high-powered field ($P = <0.001$). **h**, Neither DC population expressed detectable cytokeratin 18 mRNA. Scale bar, 15 µm (**a** and **b**), 50 µm (**c**), 25 µm (**f**). Data in **g** taken from nine or more high-powered fields (representing more than 150 cells) Data in **h** performed in triplicate and is representative of two experiments. Error bars, s.e.m. nd, not detected.

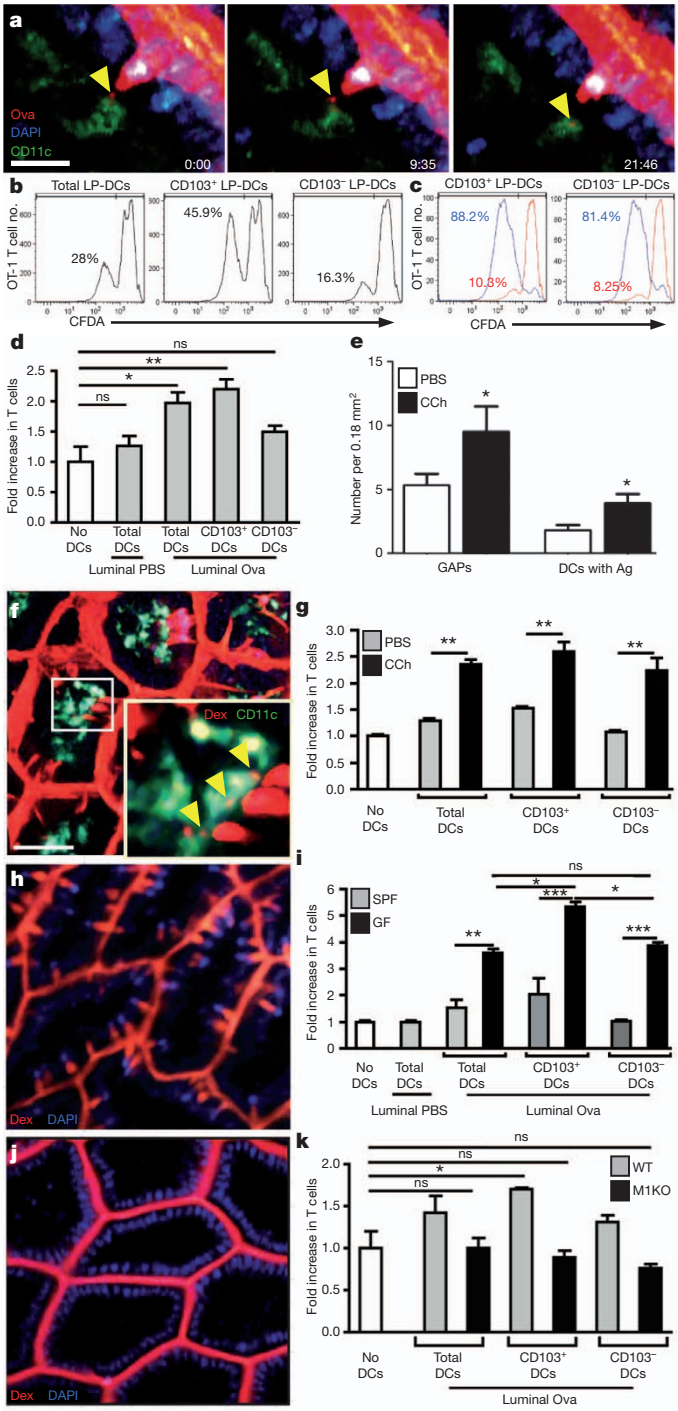

Figure 4 | GAPs are a source of luminal antigen for CD103$^+$ LP-DCs in the steady-state. **a**, Two-photon time-lapse images of a LP-DC (CD11c-YFP$^+$, green) acquiring fluorescent Ova (yellow arrow) from a GAP (red) in the intestinal epithelium (DAPI-stained nuclei, blue). Scale bar, 15 μm; time stamp, min:s of elapsed time. **b–d**, LP-DC antigen presentation capacity in mice given luminal Ova or PBS assessed on day 3 by CFDA dilution (**b**, **c**) and by counting the number of T cells after co-culture with LP-DCs (**d**). **c**, CD103$^-$ LP-DCs induced T-cell proliferation comparable to CD103$^+$ LP-DCs when exogenous antigen was added to the *in vitro* cultures (blue histogram), PBS controls (red histograms). **e**, **f**, Two-photon imaging of GAPs and LP-DCs in CCh-treated mice. CCh increased the number of GAPs and the colocalization of 10 kDa dextran (red) with LP-DCs (green). **f**, Inset, LP-DCs capturing dextran (yellow arrowheads). **g**, Luminal antigen presentation by LP-DCs following CCh administration as compared to controls given luminal Ova. **h**, Germ-free mice had increased GAPs (10 kDa dextran, red; DAPI, blue). **i**, Luminal antigen presentation by LP-DCs from germ-free mice was significantly enhanced compared to LP-DCs from SPF housed mice. CD103$^+$ LP-DCs presented luminal antigen significantly better than CD103$^-$ LP-DCs from germ-free mice. **j**, Two-photon imaging of intestines in M1KO mice. M1KO mice lacked GAPs (red, 10 kDa dextran) in the epithelium (blue, DAPI). **k**, Luminal antigen presentation by LP-DCs from M1KO mice was undetectable. Scale bar, 20 μm (**a**), 40 μm (**f**). ns, not significant. $*P < 0.05$, $**P < 0.01$, $***P < 0.001$. Error bars, s.e.m. Data in **d**, **g** and **k** are representative of three or more independent experiments, data in **i** was representative of two independent experiments. In **e**, $n = 15$ or more images were obtained from three animals for each condition.

formation, we administered the cholinergic agonist carbamylcholine (CCh) to stimulate GC secretion and imaged the small intestine by two-photon microscopy. After CCh administration, the frequency of GAPs increased markedly, as did the amount of luminal antigen colocalized with LP-DCs (Fig. 4e, f), whereas paracellular leaks or TEDs were unaffected during our imaging time-frame (Fig. 4f). Furthermore, total LP-DCs, CD103$^+$ LP-DCs and CD103$^-$ LP-DCs from CCh-treated mice significantly enhanced the luminal antigen presentation in *ex vivo* T-cell proliferation assays (Fig. 4g and Supplementary Fig. 8), indicating that GC secretion is linked mechanistically to GAP formation and luminal antigen delivery.

We also examined whether the increased number of GAPs in germ-free mice (Fig. 4h and Supplementary Fig. 2e, g) correlated with increased luminal antigen presentation by LP-DCs. LP-DCs from germ-free mice given luminal Ova showed significantly increased antigen presentation capacity compared to LP-DCs from SPF mice. Moreover, luminal antigen delivery in germ-free mice favoured CD103$^+$ LP-DCs over CD103$^-$ LP-DCs (Fig. 4i), similar to observations in SPF mice.

To test directly whether GAPs are a major pathway of antigen delivery to LP-DCs, we generated mice with an epithelial-cell-specific deletion in mouse atonal homologue 1 (Math1), a transcription factor required for the development of secretory cell lineages, including GCs[22]. Math1$^{fl/flVilCre}$ mice (M1KO) lacked small intestine GCs (Supplementary Fig. 9a–c) and *in vivo* two-photon imaging revealed a concomitant loss of GAPs, with the epithelium forming a tight barrier to luminal dextran (Fig. 4j and Supplementary Fig. 9d). Moreover, LP-DC populations isolated from M1KO mice given luminal Ova failed to stimulate OTI T cells above background levels (Fig. 4k and Supplementary Fig. 9e). The lack of antigen presentation by CD103$^+$ LP-DCs from M1KO mice was not due to an intrinsic defect, because these LP-DCs were capable of inducing robust T-cell proliferation when exogenous Ova was added to the T-cell cultures (Supplementary Fig. 9f). Taken together, these findings indicate that GAPs are a major mechanism for delivering luminal antigens to LP-DCs in the steady state.

Understanding how the balance between tolerance and immunity is achieved at the intestinal mucosa is crucial for oral vaccine development and the treatment of chronic intestinal inflammatory diseases. This study identifies GAPs as a mechanism by which CD103$^+$ LP-DCs can acquire innocuous antigens from the intestinal lumen in the steady state. How preferential antigen delivery is achieved is the focus of ongoing studies. Biased delivery could be a natural consequence of CD103$^+$ LP-DC sampling the epithelium more actively or perhaps being recruited selectively by chemoattractants released by or near GCs. GC deficiency or dysfunction in mice and humans has been linked to the development of intestinal inflammation[23–27]. Although this association has been attributed to the loss of mucins and other biologically active GC products, our findings suggest that GCs could play a key role in promoting intestinal immune homeostasis by delivering luminal antigen to tolerogenic LP-DCs.

METHODS SUMMARY

Mice and human specimens. All mice were of a C57BL/6 background unless otherwise specified. Healthy human jejunal sections were obtained from bariatric surgeries, placed in PBS containing dextran for 1 h before imaging. Procedures and protocols were carried out in accordance with the institutional review board at Washington University School of Medicine.

Two-photon microscopy. The intravital imaging preparation used in this study is similar to previously described methods[11,15] with the following differences: imaging is performed with the tissue within the peritoneal cavity, faecal material is not scraped from the mucosal surface and in some experiments atropine (1 mg kg^{-1}) was injected subcutaneously to dampen peristaltic movement of the small intestine. At this dose atropine did not affect the formation of TEDs or the detection of GAPs. Model fluorescent antigens, dextran (2–5 mg), Ova (2 mg), BSA, (2 mg) and FluoSpheres (1 ml undiluted) (all from Invitrogen) were injected into the intestinal lumen approximately 2 h before imaging. Human resection specimens were incubated in 10 μg ml^{-1} of dextran at room temperature for 1 h before imaging.

Full Methods and any associated references are available in the online version of the paper at www.nature.com/nature.

Received 1 August 2011; accepted 17 January 2012.

1. Weiner, H. L., da Cunha, A. P., Quintana, F. & Wu, H. Oral tolerance. *Immunol. Rev.* **241,** 241–259 (2011).
2. Jaensson, E. *et al.* Small intestinal $CD103^+$ dendritic cells display unique functional properties that are conserved between mice and humans. *J. Exp. Med.* **205,** 2139–2149 (2008).
3. Johansson-Lindbom, B. Functional specialization of gut $CD103^+$ dendritic cells in the regulation of tissue-selective T cell homing. *J. Exp. Med.* **202,** 1063–1073 (2005).
4. Uematsu, S. *et al.* Regulation of humoral and cellular gut immunity by lamina propria dendritic cells expressing Toll-like receptor 5. *Nature Immunol.* **9,** 769–776 (2008).
5. Varol, C. *et al.* Intestinal lamina propria dendritic cell subsets have different origin and functions. *Immunity* **31,** 502–512 (2009).
6. Schulz, O. *et al.* Intestinal $CD103^+$, but not $CX3CR1^+$, antigen sampling cells migrate in lymph and serve classical dendritic cell functions. *J. Exp. Med.* **206,** 3101–3114 (2009).
7. Bogunovic, M. *et al.* Origin of the lamina propria dendritic cell network. *Immunity* **31,** 513–525 (2009).
8. Coombes, J. L. *et al.* A functionally specialized population of mucosal $CD103^+$ DCs induces $Foxp3^+$ regulatory T cells via a TGF-β and retinoic acid-dependent mechanism. *J. Exp. Med.* **204,** 1757–1764 (2007).
9. Sun, C. M. *et al.* Small intestine lamina propria dendritic cells promote de novo generation of Foxp3 T reg cells via retinoic acid. *J. Exp. Med.* **204,** 1775–1785 (2007).
10. Niess, J. H. & Adler, G. Enteric flora expands gut lamina propria CX_3CR1^+ dendritic cells supporting inflammatory immune responses under normal and inflammatory conditions. *J. Immunol.* **184,** 2026–2037 (2010).
11. Watson, A. J. *et al.* Epithelial barrier function *in vivo* is sustained despite gaps in epithelial layers. *Gastroenterology* **129,** 902–912 (2005).
12. Hesse, M. *et al.* A mutation of keratin 18 within the coil 1A consensus motif causes widespread keratin aggregation but cell type-restricted lethality in mice. *Exp. Cell Res.* **313,** 3127–3140 (2007).
13. Hase, K. *et al.* Uptake through glycoprotein 2 of $FimH^+$ bacteria by M cells initiates mucosal immune response. *Nature* **462,** 226–230 (2009).
14. Kühn, R., Lohler, J., Rennick, D., Rajewsky, K. & Muller, W. Interleukin-10-deficient mice develop chronic enterocolitis. *Cell* **75,** 263–274 (1993).
15. Chieppa, M., Rescigno, M., Huang, A. Y. & Germain, R. N. Dynamic imaging of dendritic cell extension into the small bowel lumen in response to epithelial cell TLR engagement. *J. Exp. Med.* **203,** 2841–2852 (2006).
16. Niess, J. H. CX_3CR1-mediated dendritic cell access to the intestinal lumen and bacterial clearance. *Science* 307**,** 254–258 CrossRef (2005).
17. Rescigno, M. *et al.* Dendritic cells express tight junction proteins and penetrate gut epithelial monolayers to sample bacteria. *Nature Immunol.* **2,** 361–367 (2001).
18. Rescigno, M., Rotta, G., Valzasina, B. & Ricciardi-Castagnoli, P. Dendritic cells shuttle microbes across gut epithelial monolayers. *Immunobiology* **204,** 572–581 (2001).
19. Shen, L., Weber, C. R., Raleigh, D. R., Yu, D. & Turner, J. R. Tight junction pore and leak pathways: a dynamic duo. *Annu. Rev. Physiol.* **73,** 283–309 (2011).
20. Madara, J. L. & Trier, J. S. Structure and permeability of goblet cell tight junctions in rat small intestine. *J. Membr. Biol.* **66,** 145–157 (1982).
21. Hogquist, K. A. *et al.* T cell receptor antagonist peptides induce positive selection. *Cell* **76,** 17–27 (1994).
22. Shroyer, N. F. *et al.* Intestine-specific ablation of *Mouse atonal homolog 1* (*Math1*) reveals a role in cellular homeostasis. *Gastroenterology* **132,** 2478–2488 (2007).
23. Dvorak, A. M. & Dickersin, G. R. Crohn's disease: transmission electron microscopic studies. I. Barrier function. Possible changes related to alterations of cell coat, mucous coat, epithelial cells, and Paneth cells. *Hum. Pathol.* **11,** 561–571 (1980).
24. Eri, R. D. *et al.* An intestinal epithelial defect conferring ER stress results in inflammation involving both innate and adaptive immunity. *Mucosal Immunol.4* 354–364 (2011).
25. Trabucchi, E. *et al.* Differential diagnosis of Crohn's disease of the colon from ulcerative colitis: ultrastructure study with the scanning electron microscope. *Int. J. Tissue React.* **8,** 79–84 (1986).
26. Tytgat, K. M., van der Wal, J. W., Einerhand, A. W., Buller, H. A. & Dekker, J. Quantitative analysis of MUC2 synthesis in ulcerative colitis. *Biochem. Biophys. Res. Commun.* **224,** 397–405 (1996).
27. Van der Sluis, M. *et al.* Muc2-deficient mice spontaneously develop colitis, indicating that MUC2 is critical for colonic protection. *Gastroenterology* **131,** 117–129 (2006).

Supplementary Information is linked to the online version of the paper at www.nature.com/nature.

Acknowledgements This work was supported in part by grants DK064798 (R.D.N.), AI083538 (R.D.N.), AI095550 (R.D.N. and M.J.M.), DK085941 (L.W.W.) and AI077600 (M.J.M.). The authors thank W. Beatty for assistance with confocal microscopy, C. Eagon for assistance with human specimens, the Alvin J. Siteman Cancer Center at Washington University School of Medicine and Barnes-Jewish Hospital in St. Louis for the use of the Siteman Flow Cytometry Core, which provided high-speed flow sorting and the Washington University Digestive Disease Research Core Center (DDRCC), which provided gnotobiotic mice. The Siteman Cancer Center is supported in part by an NCI Cancer Center Support Grant number P30 CA91842. The Washington University DDRCC is supported by grant P30-DK52574.

Author Contributions J.R.M. and L.W.W. contributed equally to this work. J.R.M., B.W. and V.K. performed two-photon imaging experiments and data analysis, L.W.W., K.A.K. and K.G.M. performed cell isolation, *in vitro* studies and immunofluorescence and data analysis, R.D.N. and M.J.M. conceived of the study, directed the experimental design, analysed the data and wrote the manuscript. R.D.N. and M.J.M. contributed equally to this work and are equal corresponding authors. All authors reviewed and discussed the manuscript.

Author Information Reprints and permissions information is available at www.nature.com/reprints. The authors declare no competing financial interests. Readers are welcome to comment on the online version of this article at www.nature.com/nature. Correspondence and requests for materials should be addressed to M.J.M. (miller@pathology.wustl.edu) or R.D.N. (rnewberry@wustl.edu).

METHODS

Mice and human specimens. C57BL/6 mice, *Rag*$^{-/-}$ mice, Balb/c mice, *IL-10*$^{-/-}$ knockout mice on the C3H/HejBir.129 background[14], OTI T cell receptor transgenic mice[21], CX_3CR1-GFP knock-in mice[28], Math1$^{fl/fl}$ mice[22] and Villin Cre transgenic mice[29] were purchased from The Jackson Laboratory. CD11c-YFP transgenic mice[30] were a gift from M. Nussenzweig and LysM-GFP mice[31] were a gift from K. Ley. Gnotobiotic mice were obtained from the Washington University Digestive Disease Research Core Center murine models core. Animals, other than gnotobiotic mice, were housed in a specific-pathogen-free facility and fed routine chow diet. Animals were 8 to 16 weeks of age at the time of analysis. Intestines from mice receiving 250 rads of gamma irradiation and killed 6 h later served as positive controls for apoptosis markers. All mice were on a C57BL/6 background unless otherwise specified. Healthy human jejunal sections were obtained from bariatric surgeries, placed in PBS containing dextran for 1 h before imaging. Procedures and protocols were carried out in accordance with the institutional review board at Washington University School of Medicine.

Intravital two-photon microscopy. The intravital imaging preparation used in this study is similar to previously described methods[11,15] with the following differences: the intestine is not exteriorized during imaging, faecal material is not scraped from the mucosal surface and in some experiments atropine (1 mg kg^{-1}) was injected subcutaneously to dampen peristaltic movement of the small intestine. Mice were anaesthetized with isofluorane and a small vertical incision was made in the abdominal wall to expose the peritoneal cavity and contents. The intestine is secured to the bottom of a glass coverslip on the upper chamber plate using a thin ring of Vetbond tissue adhesive (3M). Because the coverslip sits directly over the incision in the mouse abdomen the tissue remains in the peritoneal cavity for imaging. No additional manipulations were performed to image from the serosal surface. The imaging chamber was maintained at 37 °C using a dual-channel heating system (Warner Instruments). To image from the luminal surface, a small longitudinal incision was made in the intestine taking care to avoid large blood vessels. Model fluorescent antigens, dextran (2–5 mg), Ova (2 mg), BSA (2 mg) and FluoSpheres (1 ml undiluted) (all from Invitrogen) were injected into the intestinal lumen ~2 h before imaging. Human resection specimens were incubated in 10 μg ml^{-1} of dextran at room temperature for 1 h before imaging. Time-lapse imaging was performed with a custom-built two-photon microscope running ImageWarp acquisition software (A&B Software). For time-lapse imaging, we averaged 15 video-rate frames (0.5 s per slice) during the acquisition. Each plane represents an image of 220 × 240 μm in the *x* and *y* dimensions. 21 to 31 sequential *z*-steps (2.5 μm each) were acquired to form a *z*-stack. In our experiments epithelial integrity was assessed by dextran and DAPI staining, which in healthy tissue, demarcates the luminal surface of the epithelium (aside from GAPs) and shows an ordered arrangement of DAPI-stained nuclei, respectively. In some experiments mice were given 10^8 *Salmonella typhimurium* strain χ3716 orally 24–72 h before imaging.

Flow cytometry, immunohistochemistry and confocal microscopy. Flow cytometry and the staining of intestine sections were performed as previously described[32]. Reagents used for flow cytometry include anti-CD11c, anti-CD45, anti-CD4, anti-MHCII, anti-CD3, anti-CD8a, anti-PDCA-1 (all from eBioscience), 7-aminoactinomycin D (7-AAD), anti-CD103 and anti-B220 (both from BD Biosciences). Data was acquired with a FACScan cytometer (BD Biosciences) retrofitted with additional lasers. Data acquisition was performed using CellQuest (BD Biosciences) and Rainbow (Cytek) or FlowJo software (Tree Star). Data analysis was performed on a Macintosh computer running FlowJo software.

To immobilize the lysine-fixable fluorescent dextrans, intestinal sections were treated with 2% paraformaldehyde immediately after two-photon imaging. Reagents used for immunohistochemistry include 4′,6-diamidino-2-phenylindole (DAPI; Sigma-Aldrich), anti-CD11c, anti-CD103, anti-e cadherin (all from BD Biosciences), anti-cytokeratin 18 and anti-MUC2 (both from abcam), anti-GP2 (MBL International), anti-cleaved cytokeratin 18 (Enzo Life Sciences), and anti-cleaved caspase 3 (Cell Signaling Technology). The terminal deoxynucleotidyl transferase-mediated dUTP nick end labelling (TUNEL) assay (Trevigen) was performed as per the manufacturers recommendations. Confocal microscopy was performed using a Zeiss LSM510 Meta laser scanning confocal microscope (Carl Zeiss) equipped with a ×63, 1.4 numerical aperture Zeiss Plan Apochromat oil objective. Images were obtained using the Zeiss LSM510 software.

T-cell proliferation assays. Mice were anaesthetized and the small intestine injected intraluminally with 2 mg of Ova (Sigma-Aldrich) dissolved in phosphate buffered saline (PBS), or PBS alone (controls) as in the two-photon imaging experiments. In some experiments mice received 3 μg of carbamylcholine (Sigma-Aldrich) subcutaneously 20 min after the administration of luminal Ova. Two hours after the administration of Ova, cell populations were isolated from the intestinal lamina propria as previously described[32] and sorted by flow cytometry into total LP-DC populations (7-AAD$^-$, CD45$^+$ MHCII$^+$ CD11c$^+$), CD103$^+$ DC populations (7-AAD$^-$, CD45$^+$ MHCII$^+$ CD11c$^+$ CD103$^+$), or CD103$^-$ DC populations (7-AAD$^-$, CD45$^+$ MHCII$^+$ CD11c$^+$ CD103$^-$). Sorted DC populations were cultured with sorted CFDA (Invitrogen)-labelled OTI splenic T cells at a ratio of 1:10 DC to T cells. As a positive control, 20 μg of Ova was added to cultures of DC populations isolated from mice receiving luminal PBS, unless otherwise stated. After 3 days cultures were evaluated for CFDA dilution and the number of T cells by flow cytometry and cell counting.

Real-time PCR. RNA isolation, cDNA synthesis, standard curve construction and real time PCR were performed as previously described[32]. The following primers were used: 18S, forward, 5′-CGGCTACCACATCCAAGGAA-3′ and reverse, 5′-GCTGGAATTACCGCGGCT-3′; cytokeratin 18, forward, 5′-CAGCCAGCG TCTATGCAGG-3′ and reverse, 5′-CTTTCTCGGTCTGGATTCCAC-3′. Small intestine epithelial cell populations were stained with cytokeratin 18 and AlexaFluor 488 (Invitrogen)-labelled lectin from *Ulex europaeus* (UEA-I; Sigma-Aldrich). Goblet cell populations were isolated by flow cytometric sorting as UEA-I$^+$ cytokeratin 18$^+$ cells.

Statistical analysis. Data analysis using Student's *t* test or a one-way ANOVA with a Tukey's post test were performed using GraphPad Prism (GraphPad Software).

28. Jung, S. *et al.* Analysis of fractalkine receptor CX(3)CR1 function by targeted deletion and green fluorescent protein reporter gene insertion. *Mol. Cell. Biol.* **20,** 4106–4114 (2000).
29. Madison, B. B. *et al. cis* elements of the villin gene control expression in restricted domains of the vertical (crypt) and horizontal (duodenum, cecum) axes of the intestine. *J. Biol. Chem.* **277,** 33275–33283 (2002).
30. Lindquist, R. L. *et al.* Visualizing dendritic cell networks *in vivo*. *Nature Immunol.* **5,** 1243–1250 (2004).
31. Faust, N., Varas, F., Kelly, L. M., Heck, S. & Graf, T. Insertion of enhanced green fluorescent protein into the lysozyme gene creates mice with green fluorescent granulocytes and macrophages. *Blood* **96,** 719–726 (2000).
32. McDonald, K. G., McDonough, J. S., Dieckgraefe, B. K. & Newberry, R. D. Dendritic cells produce CXCL13 and participate in the development of murine small intestine lymphoid tissues. *Am. J. Pathol.* **176,** 2367–2377 (2010).